Speckle Filtering of SAR Images - A Comparative Study Between Complex-Wavelet-Based and Standard Filters *

L. Gagnon and A. Jouan

Département de R&D, Lockheed Martin Canada, 6111 Ave. Royalmount, Montréal(Québec), H4P 1K6, CANADA

ABSTRACT

We present a comparative study between a complex Wavelet Coefficient Shrinkage (WCS) filter and several standard speckle filters that are widely used in the radar imaging community (Lee, Kuan, Frost, Geometric, Kalman, Gamma, etc.). The WCS filter is based on the use of Symmetric Daubechies (SD) wavelets which share the same properties as the real Daubechies wavelets but with an additional symmetry property. The filtering operation is an elliptical soft-thresholding procedure with respect to the principal axes of the 2-D complex wavelet coefficient distributions. Both qualitative and quantitative results (signal to mean square error ratio, equivalent number of looks, edgemap figure of merit) are reported. Tests have been performed using simulated speckle noise as well as real radar images. It is found that the WCS filter performs equally well as the standard filters for low-level noise and slightly outperforms them for higher-level noise.

Keywords: Image processing, Synthetic Aperture Radar, Speckle, Wavelets

1. INTRODUCTION

The aim of this paper is to present the results of a comparative study between a complex Wavelet Coefficient Shrinkage (WCS) filter and several custom speckle filters that are largely used by Synthetic Aperture Radar (SAR) imaging scientists. Our WCS filter is based on the use of Symmetric Daubechies (SD) wavelets, which are obtained from a complex multiresolution analysis (MRA).

The present work is part of the image analysis activities at Lockheed Martin Canada (LM Canada). The company is the prime contractor for a new Spotlight SAR (SSAR) sensor and is involved in the study, design, implementation and development of algorithms for airborne surveillance applications. In particular, these include the study of algorithms for the fusion of dissimilar data coming from imaging (SAR, FLIR) and non-imaging sensors (radar, ESM, IFF,...) in order to (1) improve long range Automatic Target Recognition (ATR) (especially ship targets) and (2) enhance Command & Control Systems[1].

1.1 Speckle

Speckle noise is a common phenomena in all coherent imaging systems like laser, acoustic and SAR imagery[2–4]. The source of this noise is attributed to random interference between the coherent returns† issued from the numerous scatterers present on a surface, on the scale of a wavelength of the incident radar wave (i.e. a resolution cell). Speckle noise is often an undesirable effect, especially for ATR systems. Thus, speckle filtering turns out to be a critical pre-processing step for detection/classification optimisation.

Basically, SAR speckle reduction techniques fall into two categories: non-coherent (or multi-look integration) and adaptive image restoration techniques (post-image formation methods). Multi-look techniques[5] consist of (1) dividing the bandwidth of the azimuth (along track) spectrum of the radar image into L segments (called looks and corresponding to L echo spectra of the same scene point generated by L incident radar pulses), (2) forming L

*SPIE Proc. #3169, conference "Wavelet Applications in Signal and Image Processing V", San Diego, 1997

†Early descriptions of speckle noise were given by optical scientists around 1962. They used to use the term "wavelets" rather than "returns", in reference to the historical Huyghens's nomenclature for the description of light propagation and diffusion.

independent images from these spectra and (3) incoherently averaging them. This reduces the azimuth spectrum bandwidth, and thus speckle noise, but at the expense of increasing the computational load and degrading the image resolution if L is too large. However, many SAR systems integrate few looks during the image formation in order to minimally improve image quality. If necessary, residual speckle has to be processed using post-image formation filters[6-14]. Among the more widely used filters are the Median, Lee, Kuan, Frost and Gamma filters. Others like the Kalman, Geometric, Oddy and AFS filters are less common (maybe because of the algorithmic complexity) but are nevertheless considered as competitive candidates to the "standard" filters. All these filters usually perform efficiently on most SAR images but with some limitations regarding resolution degradation and smoothing of uniform areas. Wavelet-based filterings have been proposed to overcome these difficulties[15-19]. They are essentially based on a WCS approach and seem to demonstrate a higher quality in image enhancement (i.e. good signal averaging over homogeneous regions with minimal resolution degradation of image details). We have recently proposed such a filter, based on the use of SD wavelets[19]. The performance results were encouraging but comparative tests were performed only with a small subset of standard filters (Median and Geometric). A more extensive test bank was required in order to better validate our tool; this is the purpose of the present work.

1.2 Speckle statistics

Fully developed speckle (i.e. when the number of scatterers is large in one resolution cell) has the characteristics of a random multiplicative noise. Under the assumption that the real and imaginary parts (respectively the so-called in-phase (denoted I) and quadrature (denoted Q) components of a complex radar image) of the speckle have zero-mean Gaussian density, noise intensity can be shown to follow a Gamma distribution (which reduces to an exponential distribution for single-look images)[5]. The mean-to-standard-deviation ratio (a measure of the signal-to-noise ratio) of such a distribution satisfies

$$\left(\frac{\text{mean}}{\text{standard deviation}}\right)^2 = L = constant \tag{1.1}$$

A usual way to estimate the speckle noise level in a SAR image is to calculate Eq. (1.1), often termed the Equivalent Number of Looks (ENL), using pixel intensity values over a uniform image area. Unfortunately, the ENL carries no information on the resolution degradation and because of that, we will use it jointly with the Signal-to-Mean-Square-Error Ratio (S/MSE) ($10log_{10}[\sum_{pixels} I_1^2 / \sum_{pixels}(I_2 - I_1)^2]$, where I_1 and I_2 are the unnoisy and noisy images, respectively) which corresponds to the standard SNR in case of additive noise.

Experimentally measured speckle distributions can deviate from the theoretical Gamma distribution for specific types of targets. For instance, Log-Normal distribution turns out to be a good speckle model for high-resolution sea-clutter imagery[20]. Because of our particular interest in ocean surveillance, we have retained this distribution in our speckle simulations. However, it appeared later that this choice is not critical (tests performed with the Gamma distribution have shown no significant change in the filter performance results). One can generate the Log-Normal distribution using

$$X_{Log-Normal} = \exp(X_{Normal}\sqrt{2\log M/m} + \ln m) \tag{1.2}$$

where M and m are the mean and median values of the distribution and $X_{Normal} \sim N(0,1)$. Without loss of generality, we have chosen $M = 1$. The equivalence between m and L has been calculated numerically and is given in Table 1.

m	0.70	0.75	0.80	0.85	0.87	0.90	0.92	0.95	0.97	0.99
L	1.0	1.4	1.9	2.7	3.2	4.4	5.6	9.4	16	50

Table 1: Number of looks L as a function of median parameter m for the Log-Normal distribution (1.2) with $M = 1$

1.3 Symmetric Daubechies wavelets

Symmetric Daubechies (SD) wavelets, and their underlying scaling functions, are obtained from a complex MRA[21,22]. The complex scaling function $\varphi(x)$ and wavelet $\psi(x)$ satisfy the usual MRA equations

$$\varphi(x) = 2\sum_k a_k \ \varphi(2x-k) \qquad \psi(x) = 2\sum_k b_k \ \varphi(2x-k) \tag{1.3}$$

with

$$a_k = a_{2J+1-k}; \qquad b_k = (-1)^k a^{\star}_{2J+1-k} \quad J = 0, 2, 4, 6, ... \quad k = 0, ..., 2J+1 \tag{1.4}$$

where $\star$ stands for complex conjugate.

In addition to sharing the same properties as the real Daubechies wavelets (i.e. compact support, orthogonality and vanishing moments), SD wavelets and scaling functions are symmetric (respectively of odd and even parity with respect to the center of the compact support) and have a better interpolation capability due to identical vanishing of the second centered moment of the real part of the scaling function[23]. Multiwavelets can also hold concurrently all these properties[24] and in fact, as is obvious from Eq. (1.3), SD wavelets also have a multi-wavelet interpretation in terms of 2x2 matrices.

Symmetry is the property that makes SD wavelets particularly interesting for image processing applications. It allows the use of symmetric extension of data at the image boundaries. Symmetric extension prevents discontinuities introduced by a periodic wrapping of the data. Apart from slightly increasing the computational load, the complex-value of the transform is not really a drawback (Fourier transform is also complex!). Like Fourier, SD wavelets introduce redundancy in the transformation of a real signal but this can be used in an advantageous way for the design of local multiresolution sharpening operators and POCS (Projection Onto Convex Sets) filtering algorithms[23,25]. Also, it has been experimentally demonstrated that phase of the wavelet coefficients encodes much information on edges[25].

2. SPECKLE FILTERS

2.1 Wavelet filter

Our wavelet speckle filter is based on the well-known soft-thresholding procedure[26]. However, use of SD wavelets provides an opportunity to modify this algorithm in order to manage the complex-valued characteristic.

We have numerically observed that wavelet coefficients in each spectral band (the so-called VW, WV and WW blocks) can be modelized as a bi-Normal distribution of mean (μ_x, μ_y) (nearly zero) and covariance matrix R which is in general not diagonal (real and imaginary parts are correlated). In addition, the distributions are usually oriented differently in each block (Figure 1). Based on this fact, it seemed natural to us to propose an algorithm that performs wavelet coefficients thresholding with respect to the principal axes (ξ, η) of the 2-D distributions. As a result, the threshold level becomes angle-dependent and extends in proportion to the eccentricity of the centered dispersion ellipse. In practice, since the noise characteristics can differ in each block, we have also chosen to process them separately. Thus, the VW block at the highest resolution level provides noise statistics for thresholding all the lower resolution VW blocks (similarly for the WV and WW blocks).

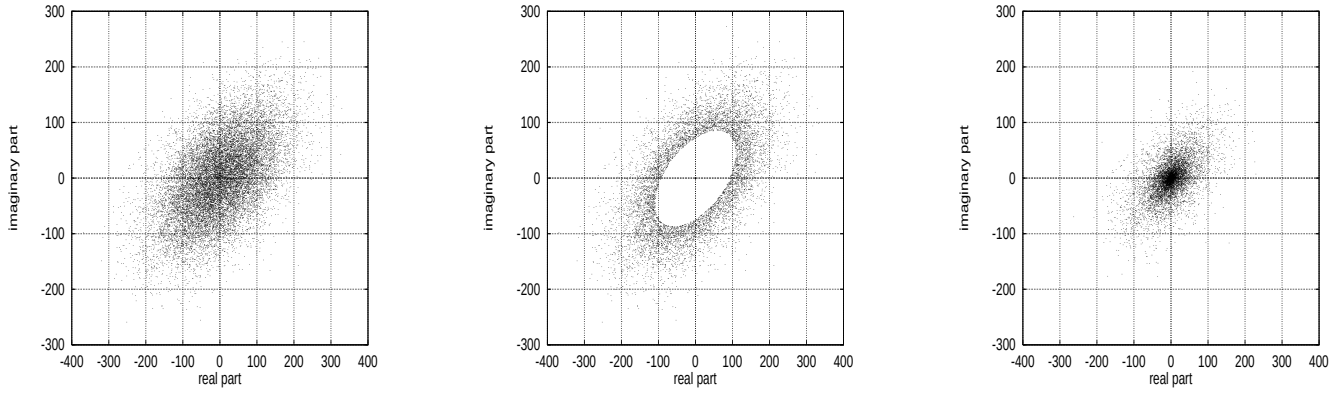

Figure 1: Illustration of the elliptical thresholding rule on a complex wavelet coefficient distribution. Left: before thresholding. Center: elliptical thresholding area. Right: after thresholding

The complete WCS for SAR image then proceeds as follows[19].

- Make a logarithmic transformation (more precisely $\log(I+1.0)$) of the original image I
- Make a N-level SD wavelet transform
- For each block type (VW, WV and WW) and level j (j=1,2,...,N), perform the following operations:
  - Calculate the mean, covariance matrix elements, orientation angle and uncorrelated standard deviations σ_ξ and σ_η of the wavelet coefficient distribution
  - Noting $w_k \equiv \xi + i\eta$ (with respect to the principal axis coordinates), apply the following elliptical soft-thresholding rule

$$|w_k| \to 0 \quad \text{if} \quad \frac{\xi^2}{t_\xi^2} + \frac{\eta^2}{t_\eta^2} \leq 1.0 \qquad |w_k| \to |w_k| - T(\theta) \quad \text{if} \quad \frac{\xi^2}{t_\xi^2} + \frac{\eta^2}{t_\eta^2} > 1.0 \tag{2.1}$$

where

$$T(\theta) = \frac{t_\xi t_\eta}{\sqrt{(t_\xi \sin\theta)^2 + (t_\eta \cos\theta)^2}}; \qquad t_\xi = \delta\sigma_\xi^1 \qquad t_\eta = t_\xi \sigma_\eta / \sigma_\xi \tag{2.2}$$

θ is the phase of the wavelet coefficient distribution (with respect to the principal axes), σ_ξ^1 is the principal standard deviation along the ξ-axis at the finest resolution level and δ is a free denoising parameter.

- Invert the DWT
- Invert the logarithmic transformation

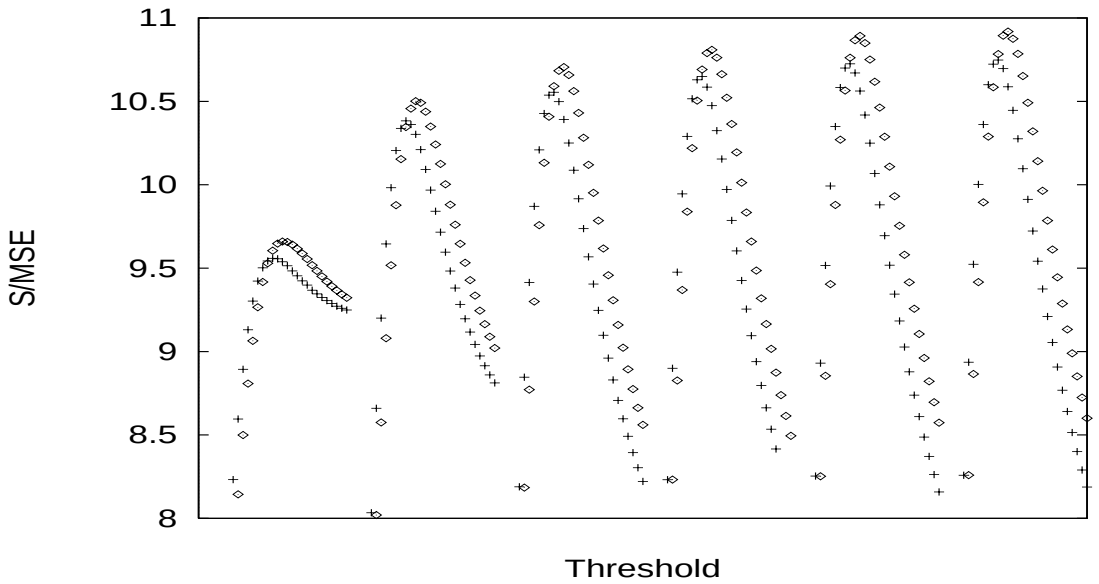

Figure 2: Variation of the S/MSE as function of δ and for $N = 1, ..., 6$ (see text for details)

The logarithm transformation is a common homomorphic transformation performed on SAR images and is used to transform multiplicative noise into additive noise[3]. It also allows compliance with the additive noise hypothesis in the standard WCS algorithm[26].

In order to minimize the image artifacts (Gibbs-like phenomena) resulting from the lack of translation invariance of discrete wavelet bases, we have embeded our algorithm into the cycle spinning algorithm[27]. This consists in averaging the result of the WCS filter over all possible shifts of the input image (16 translations were sufficient in practice).

Most of the numerical tests have been done with the $J = 2$ wavelet. Its short support (6-taps) minimizes the computation time and no significant changes are obtained with higher-order wavelets. Parameters N and δ have been varied during the tests (1 to 6 and 0.1 to 3.0, respectively) in order to have a clear picture of their effects. In theory, N should be large but in practice we have limited the number of decomposition levels to 6. Figure 2 shows the SMSER obtained after processing an urban image corrupted by a simulated 4.4 dB Log-Normal noise ($L = 2.7$). Each curve corresponds to a different value of N (1 to 6). Upper curves (diamonds) are for SD wavelets while lower ones (crosses) are for the 6-taps real Daubechies wavelet (with periodic warping of boundary data). Points on each curve are for different values of δ. In this case, an optimal S/MSE is obtained for $N = 6$ and $\delta = 1.4$. All the comparative results presented in the next section are for optimal S/MSE values only.

2.2 Standard filters

Let x be an image pixel corrupted by a stationary multiplicative noise n such that $y = nx$. Without loss of generality, we assume noise of unit-mean ($\bar{n} = 1$). Many standard filters require knowledge of $\bar{y}$ as well as the standard deviations σ_y and σ_n. In practice, $\bar{y}$ and σ_y are estimated locally, within a finite size window. Noise standard deviation σ_n (and L) is given as an input filter parameter or can be estimated over a uniform area in the image. In fact, under the unit-mean noise assumption, we have $ENL = (\bar{y}/\sigma_y)^2 = 1/\sigma_n^2$.

The 8 standard speckle filters considered in this comparative study are the following.

Kuan filter

The Kuan filter is based on a Minimum Mean Square Error (MMSE) criterion[8]. A MMSE estimate is first developed for and additive noise model $y = x + n$. The multiplicative noise model is then considered under the form $y = x + (n-1)x$ from which the corresponding linear filter is deduced. The Kuan filter is optimal when both the scene and the detected intensities are Gaussian distributed. Under the unit-mean noise assumption, the pixel value estimate $\hat{x}$ is given by

$$\hat{x} = \bar{y} + \frac{\sigma_x^2 (y - \bar{y})}{\sigma_x^2 + (\bar{y}^2 + \sigma_x^2)/L} \qquad \sigma_x^2 = \frac{L\sigma_y^2 - \bar{y}^2}{L+1} \tag{2.3a,b}$$

We have put $\hat{x} = \bar{y}$ for the pathological cases where measures yield $\sigma_x^2 < 0$.

Lee filter

The Lee filter (more precisely Lee MMSE filter[6]) is a particular case of the Kuan filter when the term σ_x^2/L is removed in Eq. (2.3a). This term does not appear in Lee's original derivation due to a linear approximation made there for the multiplicative noise model (a first-order Taylor series expansion of y about x and n).

Another filter that is a particular case of Kuan is the Nathan filter[9]. This one is obtained by puting $L = 1$ in Eq. (2.3) and is thus applicable to 1-look SAR images only. For this reason, it has not been included in our tests.

Gamma filter

The Gamma filter is a Maximum A Posteriori (MAP) filter based on a Bayesian analysis of the image statistics[13]. It assumes that both the radar reflectivity and the speckle noise follow a Gamma distribution. The "superposition" of these distributions yields a K-distribution which is recognized to match a large variety of radar return distributions of land and ocean targets. The estimate $\hat{x}$ is given by

$$\hat{x} = \frac{(\alpha - L - 1)\bar{y} + \sqrt{\bar{y}^2(\alpha - L - 1)^2 + 4\alpha L y \bar{y}}}{2\alpha} \qquad \alpha = \frac{L+1}{L(\sigma_y/\bar{y})^2 - 1} \tag{2.4}$$

We have put $\hat{x} = \bar{y}$ for the pathological cases where measures yield a negative or a complex estimate for $\hat{x}$.

Frost filter

The Frost filter[7] is an adaptive Wiener filter which convolves the pixel values within a fixed size window with an exponential impulse response m given by

$$m = exp[-KC_y(t_0)|t|] \qquad C_y = \sigma_y/\bar{y} \tag{2.5}$$

where K is the filter parameter, t_0 represents the location of the processed pixel and $|t|$ is the distance measured from pixel t_0. This response results from an autoregressive exponential model assumed for the scene reflectivity x.

Kalman filter

A 2D Kalman filter has been implemented on a causal prediction window, the so-called Non-Symmetric Half Plane (NSHP), defined as $W = \{p, q : 1 \leq p \leq M, -M \leq q \leq M; p = 0, 1 \leq q \leq M\}$, with $M = 2$. In this filter, the image is assumed to be represented by a Markov field which satisfies the causal autoregressive (AR) model

$$x(m,n) = \sum_{(p,q)\in W} a_{pq}\, x(m-p, n-q) + u(m,n) \tag{2.6}$$

where $x(m,n)$ represents the pixel value at location (m,n), $u(m,n)$ is a noise sequence (this is not the speckle noise) which drives the Markov process and a_{pq} are the reflection coefficients of the AR model. The parameters a_{pq} are evaluated based upon the global estimates of the autocorrelation sequence of the image over the finite window W. From these parameters, the AR model can be arranged into a 2D block recursive form (Figure 3) for the Kalman filter equations. Implementation of this filter is very much involved and we refer to Ref. 14 for more details about the 2D kinematic model (limited here to speckle modelling only) and the Kalman filter equations.

Geometric filter

The geometric filter is a nonlinear morphological filter that uses the concept of image graph[12]. The image graph is obtained by transforming the original image into a 3-dimensional diagram where the pixel coordinates specify the position of the pixel on a plane and the pixel value specifies the elevation of the pixel with respect to that plane. The filtering process itself is performed first on row slices (i.e. 1-dimensional profile graphs similar to Figure 4a) of the image graph using a 8-hulling algorithm. Slice pixels are set to 1 if the pixel is on or below the image graph surface, while pixels above the image graph surface are set to 0 (Figure 4b). The filtering algorithm searches for 4 different configurations (3x3 binary morphological masks) and when it finds one, the graph pixel corresponding to the central pixel of the mask is set to 0. The procedure is repeated for the complementary graphs and masks (Figure 4c) except that the central pixel is now incremented by 1. The whole procedure is repeated on column and diagonal slices. This completes one iterative step of the geometric filter. A filtering is achieved because speckle appears as narrow walls and valleys on the binary slice images and because the geometric filter, through iterative repetition, gradually tears down and fills up these features.

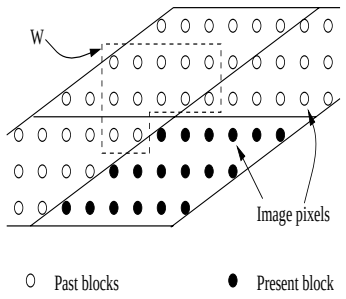

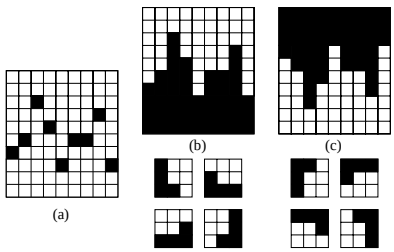

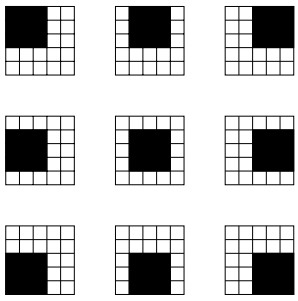

Figure 3 (left): 2D block recursive form for the Kalman filter
Figure 4 (center): (a) Exemple of image graph; (b) Binary slice and masks and their complements (c)
Figure 5 (right): The 8 binary masks used by the ASF filter

Oddy filter

The Oddy filter can be considered as a mean filter whose window shape varies according to the local statistics[10]. The estimate $\hat{x}$ is given by

$$\hat{x} = \bar{y} \quad \text{if} \quad m < \alpha\bar{y}; \qquad \hat{x} = \frac{\sum_k \sum_l W_{kl}\, y(k,l)}{\sum_k \sum_l W_{kl}} \quad \text{if} \quad m > \alpha\bar{y} \tag{2.7}$$

$$W_{kl} = 1 \quad \text{if} \quad |y(k,l) - y| \leq m; \qquad W_{kl} = 0 \quad \text{otherwise}$$

where $\bar{x}$ is evaluated locally over a 3x3 window, $m = 1/8 \sum_k \sum_l |y(k,l) - y|$ and α is the filter parameter. W plays the role of an adaptive binary mask that is applied over the window.

AFS filter

AFS filter stands for Adaptive Filter on Surfaces[11]. It is another adaptive mask filter that uses the concept of "local emerging surface" (l.e.s.) value. The l.e.s. is the area of the image graph surface defined over the window. The l.e.s. is calculated for the 9 binary masks shown in Figure 5. The mask whose l.e.s. is a minimum is selected and a mean filtering is performed over the mask pixels. The mean value is assigned to the central pixel of the 5x5 window.

3. TESTS AND DISCUSSION

3.1 Simulated images

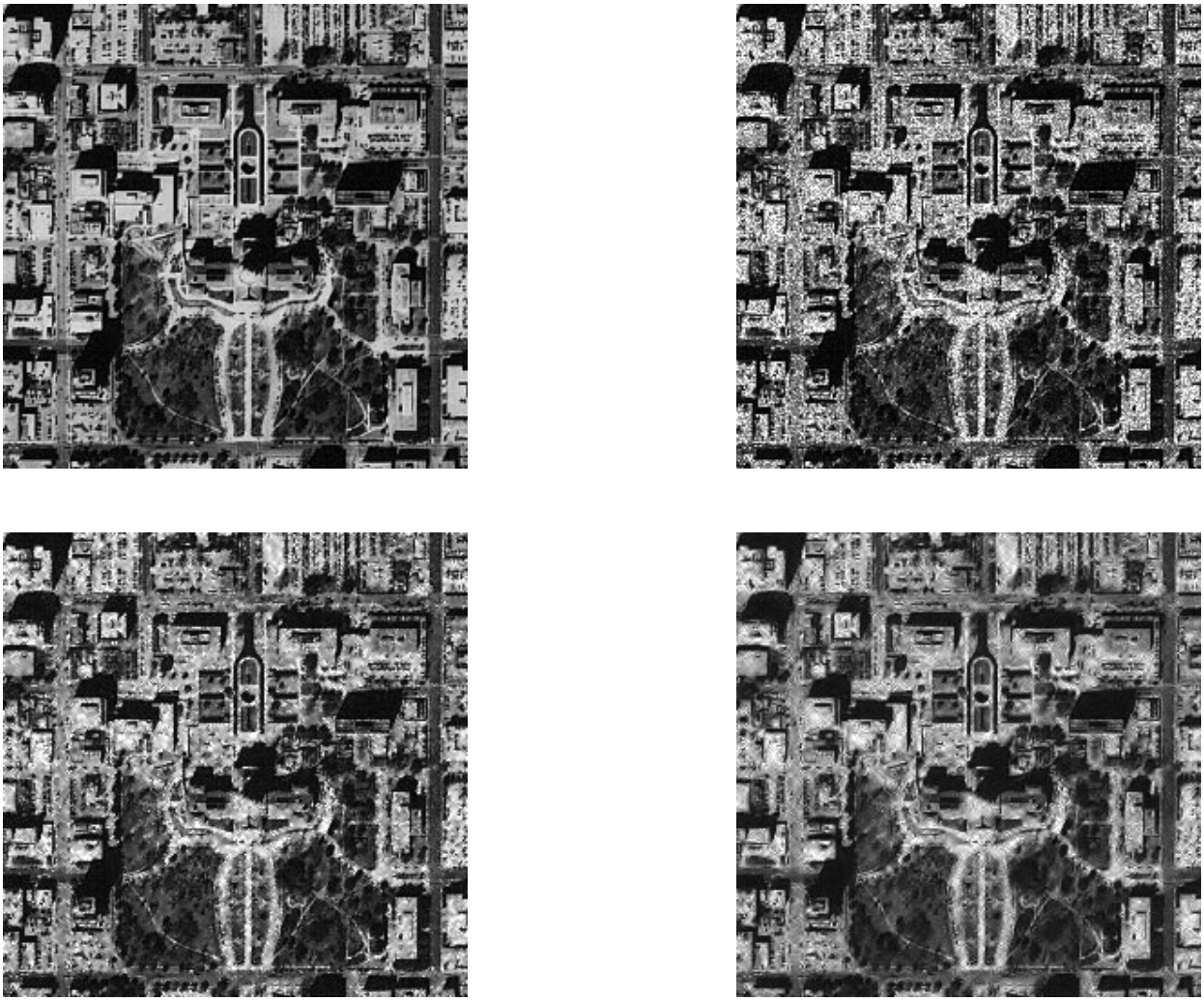

Figure 6: Urban test images.
Upper row: original and noisy ($L = 9.4$). Lower row: Gamma and Wavelet filtered (Table 2)

We have simulated radar textured images by degrading two aerial photographs (www.cent.org) with unit-mean Log-Normal multiplicative noise (Figures 6a,b and 7a,b). The two scenes (urban and agricultural regions) have

very different spectral content (high and low frequency, respectively) in order to observe the effect on the filters' performance. Three noise levels have been tested, corresponding to $L = 2.7$, 9.4 and 50. Filtering performance has also been calculated using measured ENL, as it is done in practical situations. A uniform area has been identified in each image from which ENL (or noise variance) has been measured and used in the filter equations. Quantitative performance measures are summarized in Tables 2 and 3 and correspond to the best enhanced images obtained, with respect to the S/MSE. During measures, image radiometry (image intensity) has been conserved by assuring that the enhanced and noisy images have the same global mean. Two of the best enhanced images for the case $L = 9.4$ are shown on Figures 6c,d and 7c,d.

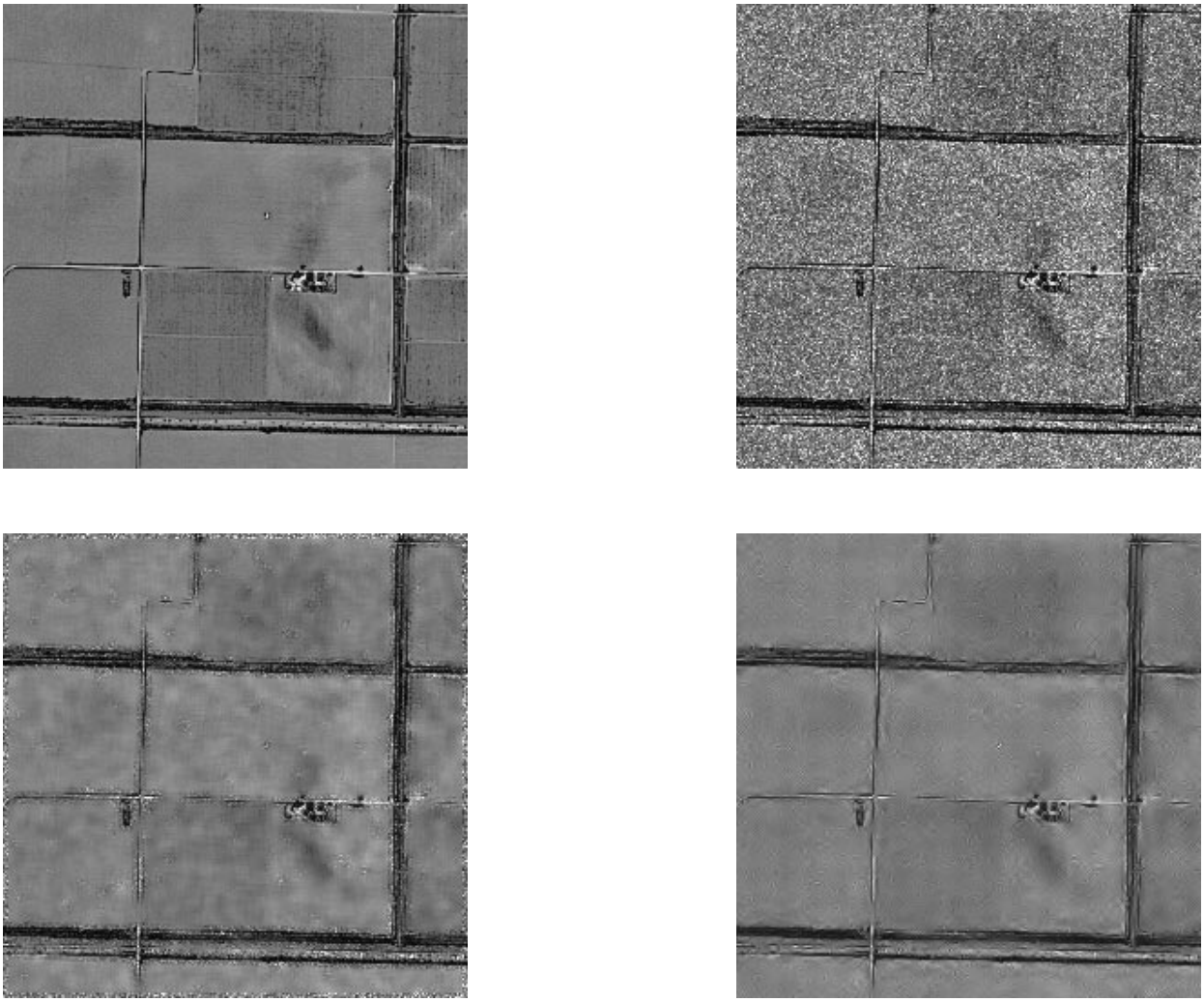

Figure 7: Agricultural test images.
Upper row: original and noisy ($L = 9.4$). Lower row: Gamma and Wavelet filtered (Table 3)

We observe from Tables 2 and 3 that the optimal S/MSE is highly dependent on the noise level and signal content. High spectral content images require lower wavelet coefficient threshold values. Higher wavelet coefficient thresholds are necessary for higher noise levels because of the more important wavelet coefficient distribution spreading.

Quantitatively, the WCS filter performs as well as the best standard filters (Frost, Gamma, Kuan) for low-level speckle noise ($L > 10$) and slightly outperforms them for higher speckle noise level ($L < 10$), especially in the case of low spectral content (Figure 7). This is verified for specific wavelet filter parameter values. Qualitatively, the wavelet filter offers the best trade-off between image resolution conservation and averaging over uniform regions. This can be

	$L = 2.7$			$L = 9.4$			$L = 50$		
	S/MSE (dB)	ENL	Notes	S/MSE (dB)	ENL	Notes	S/MSE (dB)	ENL	Notes
Noisy	4.4			9.8			17.0		
Lee	9.0	144	5x5	12.8	97	3x3	18.5	446	3x3
Kuan	9.4	144	5x5	13.0	97	3x3	18.5	448	3x3
Gamma	9.6	140	5x5	13.1	96	3x3	18.6	448	3x3
Frost	10.2	127	7x7; $K_{1.5}$	13.4	84	3x3; $K_{3.0}$	18.7	386	3x3; $K_{7.0}$
Kalman	-	-		11.7	39		-	-	
Geometric	7.9	144	3 iter.	11.6	93	2 iter.	17.5	206	1 iter.
Oddy	10.0	47	5x5; $\alpha_{0.7}$	12.9	110	3x3; $\alpha_{0.5}$	16.6	367	3x3; $\alpha_{0.2}$
AFS	8.3	37		9.4	86		10.7	433	
Wavelet	10.9	151	N_6; $\delta_{1.4}$	13.6	172	N_6; $\delta_{0.8}$	18.6	340	N_6; $\delta_{0.3}$

Table 2: Quantitative enhancement measures performed on the urban test image (Figure 6)

	$L = 2.7$			$L = 9.4$			$L = 50$		
	S/MSE (dB)	ENL	Notes	S/MSE (dB)	ENL	Notes	S/MSE (dB)	ENL	Notes
Noisy	4.3			9.7			17.0		
Lee	13.6	68	7x7	17.3	129	7x7	21.9	310	7x7
Kuan	14.0	74	7x7	17.4	140	7x7	21.9	319	7x7
Gamma	14.1	80	7x7	17.5	146	7x7	22.0	373	7x7
Frost	14.6	156	7x7; $K_{1.0}$	17.4	155	7x7; $K_{3.0}$	22.1	313	7x7; $K_{7.0}$
Kalman	-	-		15.8	63		-	-	
Geometric	13.8	471	4 iter.	16.1	555	3 iter.	20.8	218	1 iter
Oddy	14.3	89	7x7; $\alpha_{0.8}$	16.9	146	7x7; $\alpha_{0.5}$	20.6	370	3x3; $\alpha_{0.3}$
AFS	12.2	29		14.8	90		17.2	270	
Wavelet	16.3	241	N_6; $\delta_{2.0}$	18.6	345	N_6; $\delta_{1.6}$	22.1	427	N_6; $\delta_{0.8}$

Table 3: Quantitative enhancement measures performed on the agricultural test image (Figure 7)

observed, in particular, on the enhanced urban images (Figure 6). This also happens to be observed in the following experiment about edge preservation measure.

3.2 Edge map

An edge map is a binary image identifying pixels that are on an edge. In order to get a quantitative evaluation of edge preservation for each filter, we have performed an experiment proposed by Frost et al.[7]. The following procedure has been used to create an edge map under a controlled environment (1) simulate an artificial noisy edge (a 200-50 pixel intensity step here), (2) apply the filter, (3) apply a Robert's gradient operator for edge detection, (4) create a binary image by thresholding the pixel values and (4) calculate an edge map Figure Of Merit (FOM).

The edge FOM used here is the one proposed by Abdou and Pratt[28]. Let two congruent images I and A, represent ideal and actual edge maps of a single step edge. The ideal edge map is assumed to contain N_I edge pixels, while the actual edge map contains N_A. If d is the perpendicular distance from the actual edge pixel to the ideal edge, one can define a FOM by

$$R(\%) = \frac{100}{max(N_A, N_I)} \sum_{i=1}^{N_A} \frac{1}{1 + \beta d^2} \tag{3.1}$$

where β is an arbitrary penalty parameter for offset edge pixels (we choose $\beta = 10$ here). A perfect edge map yields $R = 100\%$. Since the selection of the threshold greatly affects the nature of the edge map, the threshold that yields

the optimal FOM has been determined. We have performed FOM measures on a highly ($L = 1.9$) and moderatly noisy edge ($L = 9.4$). Table 4 gives the FOM obtained when optimizing the S/MSE over the various filter parameters. The window size has been limited to 5x5 for the Lee, Kuan Gamma and Frost filters, in order to limit the resolution degradation. Four iterations have been used for the geometric filter. The WCS filter provides the best quantitative and qualitative (Figure 8) results for the noisiest case ($L = 1.9$). The difference is less important for the low-level case.

	Noisy	Lee	Kuan	Gamma	Frost	Geometric	Oddy	Wavelet
FOM(%) @ $L = 1.9$	0.9	6.1	6.4	6.2	28.2	18.3	10.9	38.1
FOM(%) @ $L = 9.4$	3.7	49.5	49.6	55.0	58.6	58.5	44.4	64.1

Table 4: Edge map FOM from Eq. (3.1) for various filters (see Figure 8 and text for details)

Figure 8: Noisy image and edge maps for the noisy Frost, Geometric and Wavelet filtered images (Table 4)

3.3 A real image

Finally, we have tested the various filters on a real high resolution (1m/pixel) strip-map SAR image obtained from an airborne platform (www.amps.gov). Figure 9 shows a portion of the original image (ENL=3, $\sigma_n^2 = 0.33$) and the enhancement produced by the Frost (7x7 window, $K = 1$), Kuan (7x7 window), Oddy (7x7 window, $\alpha = 1.0$), Gamma (7x7 window) and Wavelet filter ($N = 6$, $\delta = 2.0$). The superiority of the wavelet filter is perhaps more obvious here. Although qualitative evaluation is highly subjective, it appears that the wavelet-based filter provides a better image resolution conservation.

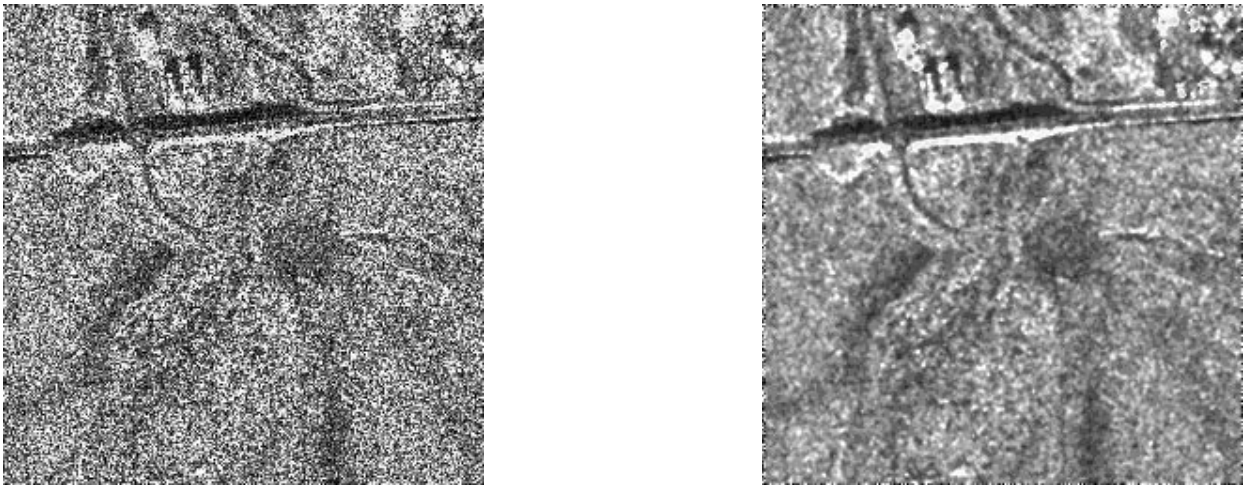

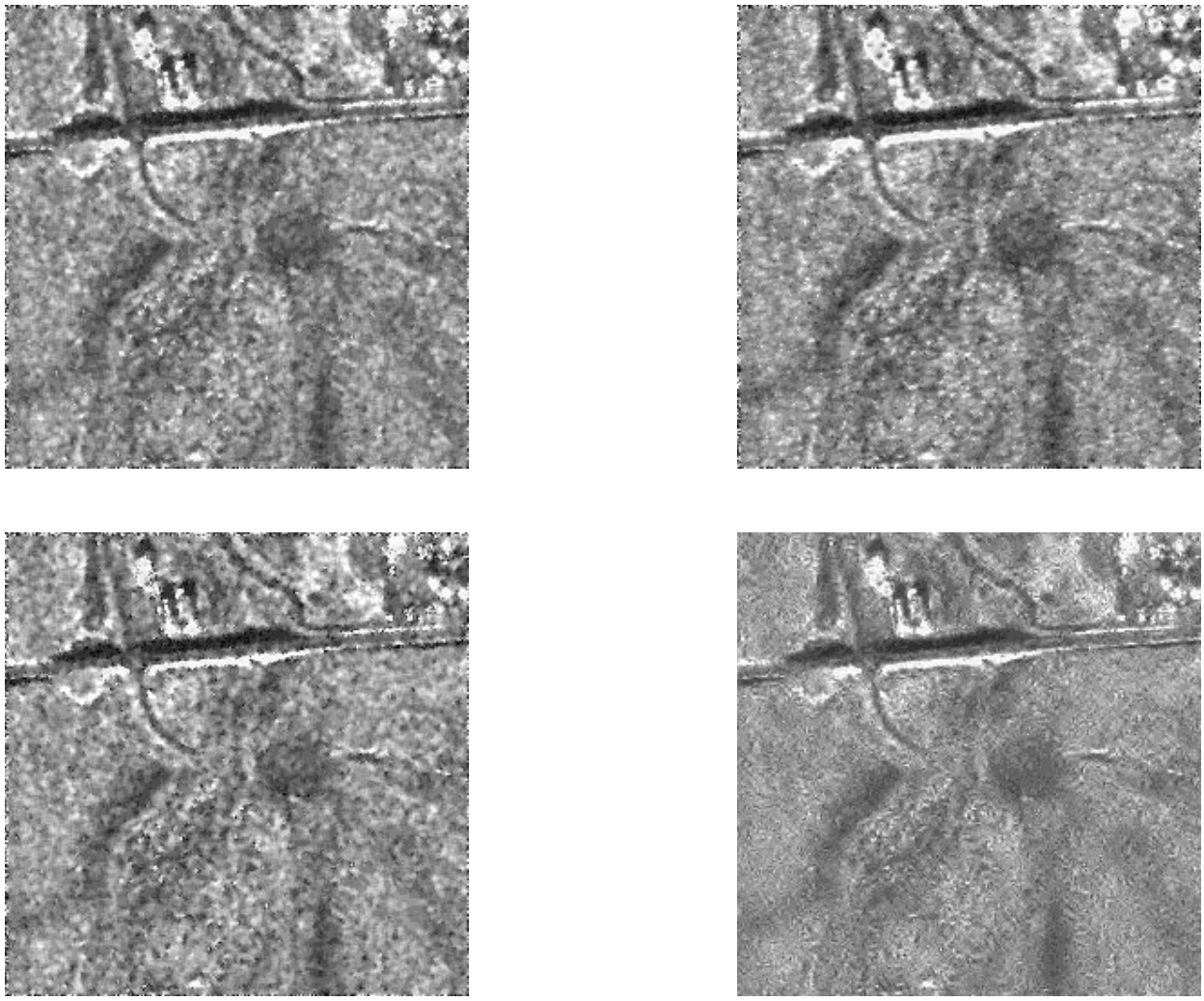

Figure 9: Noisy, Frost, Kuan, Oddy, Gamma and Wavelet enhancement for a real SAR image

4. CONCLUSIONS

We have presented a comparative study between a complex Wavelet Coefficient Shrinkage (WCS) filter and several standard speckle filters that are widely used in the radar imaging community (Lee, Kuan, Frost, Geometric, Kalman, Gamma, etc.). The WCS filter is based on the use of Symmetric Daubechies (SD) wavelets. There are two advantages in using SD wavelets: (1) symmetric extension prevents discontinuities introduced by a periodic wrapping of the data and (2) identical vanishing of the second centered moment of the real part of the scaling function provides better approximation at sampling points.

Our comparative tests with 8 standard speckle filters have shown that our WCS wavelet-based filter is among the best speckle filters. This filter quantitatively performs equally well for low-level noise ($L > 10$) and slightly outperforms standard ones (Lee, Kuan, Frost, Gamma, etc.) for higher speckle noise level ($L < 10$). Up to 10% improvement has been measured on a low spectral content image. The current drawback is that computational load might necessitate specialized hardware for real-time applications; processing of a 512x512 images takes about 3 min. on a Pentium 90 (the size of strip-map mode SAR images can easily exceed 4000x4000 pixels). Also, in practice, the theoretical threshold for wavelet coefficient shrinkage does not necessarily lead to the optimal signal-to-noise ratio for the enhanced image. A robust threshold estimator is still needed in order to automate the filtering process.

5. REFERENCES

[1] E. Shahbazian, L. Gagnon, J.-R. Duquet, M. Macieszczak, P. Valin, "Fusion of Imaging and Non-Imaging Data for Surveillance Aircraft", SPIE Proc. #3067, 1997

[2] J. W. Goodman, "Some Fundamental Properties of Speckle", J. Opt. Soc. Am., Vol. 66, pp. 1145-1150, 1976

[3] H. H. Arsenault, G. April, "Properties of Speckle Integrated with a Finite Aperture and Logarithmically Transformed", J. Opt. Soc. Am., Vol. 66, pp. 1160-1163, 1976

[4] J. S. Lim, H. Nawab, "Techniques for Speckle Noise Removal", Opt. Engineering, Vol. 20, pp. 472-480, 1981

[5] D. R. Wehner, *High-Resolution Radar*, 2nd edition (Artech House, Boston, 1994)

[6] J.-S. Lee, "Digital Image Enhancement and Noise Filtering by Use of Local Statistics", IEEE Transactions on Pattern Analysis and Machine Intelligence, Vol. PAMI-2, pp. 165-168, 1980

[7] V. S. Frost, J. A. Stiles, K. S. Shanmugan, J. C. Holtzman, "A Model for Radar Images and Its Application to Adaptive Digital Filtering of Multiplicative Noise", IEEE Transactions on Pattern Analysis and Machine Intelligence, Vol. PAMI-4, pp. 157-166, 1982

[8] D. T. Kuan, A. A. Sawchuk, T. C. Strand, P. Chavel, "Adaptive Noise Smoothing Filter for Images with Signal-Dependent Noise", IEEE Transactions on Pattern Analysis and Machine Intelligence, Vol. PAMI-7, pp. 165-177, 1985

[9] K. S. Nathan and J. C. Curlander, "Speckle Noise Reduction of 1-Look SAR Imagery", Proc. IGARSS '87 Symposium, pp. 1457-1462, 1987

[10] C. J. Oddy, A. J. Rye, "Segmentation of SAR Images using a Local Similarity Rule", Pattern Recognition Letters, Vol. 1, pp. 443-449, 1983

[11] L. Alparone, F. Boragine, S. Fini, "Parallel Architectures for the PostProcessing of SAR Images", SPIE Proc. #1360, pp. 790-802, 1990

[12] T. R. Crimmins, "Geometric Filter for Speckle Reduction", Appl. Optics, Vol. 24, pp. 1438-1443, 1985

[13] A. Lopes, E. Nezry, R. Touzi, H. Laur, "Structure Detection and Statiscal Adaptive Speckle Filtering in SAR Images", Int. J. Remote Sensing, Vol. 14, pp. 1735-1758, 1993

[14] M. R. Azimi-Sadjadi, S. Bannour, "Two-Dimensional Adaptive Block Kalman Filtering of SAR Imagery", IEEE Trans. Geosci. and Remote Sensing, Vol. 29, pp. 742-753, 1991

[15] T. Ranchin, F. Cauneau, "Speckle Reduction in Synthetic Aperture Radar Imagery Using Wavelets", SPIE Proc. #2034, pp. 432-441, 1993

[16] J. E. Odegard, H. Guo, M. Lang, C. S. Burrus, R. O. Wells Jr., L. M. Novak, M. Hiett, "Wavelet Based SAR Speckle Reduction and Image Compression", SPIE Proc. #2487, pp. 259-271, 1995

[17] H. Guo, J. E. Odegard, M. Lang, R. A. Gopinath, I. W. Selesnick and C. S. Burrus,"Wavelet Based Speckle Reduction with Application to SAR Based ATD/R", IEEE Proceedings of ICIP '94, pp. 75-79, 1994

[18] K. Lebart, J.-M. Boucher, "Speckle Filtering by Wavelet Analysis and Synthesis", SPIE Proc. #2825, 644-651 (1996)

[19] L. Gagnon, F. Drissi Smaili, "Speckle Noise Reduction of Airborne SAR Images with Symmetric Daubechies Wavelets", SPIE Proc. #2759, pp. 14-24, 1996

[20] H.-C. Shyu, Y.-S. Sun and W.-H. Shen, "The Analysis of Scan-to-Scan Integration Techniques for Sea Clutter", IEEE Proc. Nat. Radar Conf., pp. 228-233, 1994

[21] W. Lawton, "Application of Complex Valued Wavelet Transforms to Subband Decomposition", IEEE Trans. Signal Proc., Vol. 41, pp. 3566-3568, 1993

[22] J. M. Lina and M. Mayrand, "Complex Daubechies Wavelets", App. Comp. Harmonic Anal., vol. 2, pp. 219-229, 1995

[23] J. M. Lina and L. Gagnon, "Image Enhancements with Symmetric Daubechies Wavelets", SPIE Proc. #2569, pp. 196-208, 1995

[24] V. Strela, P. N. Heller, G. Strang, P. Topiwala, C. Heil, "The Application of Multiwavelet Filter Banks to Image Processing", submitted IEEE Trans. on Image Processing

[25] P. Drouilly, M.Sc. Thesis, Département de Physique, Univ. de Montréal, 1996

[26] D. L. Donoho and I. M. Johnstone, "Adapting to Unknown Smoothness via Wavelet Shrinkage", Tech. Report #425, Statistics Dept., Stanford Univ., 1993

[27] R. R. Coifman, D. L. Donoho, "Translation-Invariant De-Noising", in *Wavelets and Statistics*, Anestie Antoniadis Ed., Springer-Verlag Lecture Notes, 1995

[28] I. E. Abdou, W. K. Pratt, "Quantitative Design and Evaluation of Enhancement/Thresholding Edge Detectors", Proc. IEEE, Vol. 67, pp. 753-763, 1979